Electronic Supplementary Material (ESI) for Soft Matter.

Supporting information of

Entrapment of Interfacial Nanobubbles on Nano-Structured Surfaces

Yuliang Wang*,[1], Xiaolai Li[1], Shuai Ren[1], Hadush Tedros Alem[1], Lijun Yang[2], and Detlef Lohse*,[3,4]

[1]School of Mechanical Engineering and Automation, Beihang University, Beijing 100191, P.R. China
[2]Physics of Fluids Group, Faculty of Science and Technology, J. M. Burgers Centre for Fluid Dynamics, University of Twente, P.O. Box 217, 7500 AE Enschede, The Netherlands
[3]Max Planck Institute for Dynamics and Self-Organization, Am Fassberg 17, 37077 Göttingen, Germany
[4]School of Astronautics, Beijing University of Aeronautics and Astronautics, Beijing 100191, China

Methods

Sample preparation

The polystyrene (PS) surfaces used for nanobubble (NB) nucleation were prepared by spin coating thin films of PS on silicon (100) substrates. Before spin coating, the substrates were sequentially cleaned in sonication bathes of piranha, acetone, and then water. PS particles (molecular weight 350 000, Sigma-Aldrich) were dissolved in toluene (Mallinckrodt Chemical) to make the PS solutions.

Three PS surfaces (sample 1, sample 2, and sample 3) were prepared to obtain nanopits with different sizes and shapes. The PS concentrations for the three samples were 0.05%, 0.1%, and 0.05% (all weight), respectively. The selected speeds of spin coating for the three samples were 200 rpm,1000 rpm, and 500 rpm, respectively.

Two types of nanostructures, namely nanopits and nanopores, were fabricated on the three samples to study NB nucleation. First, on *nanopits*: For spin coated PS films, the decreasing thickness will cause inhomogeneous coating of the films[1, 2]. By delicately controlling the PS solution concentration and spin speed during spin coating, nanopits of different sizes were spontaneously obtained on sample 1 and sample 2.

On sample 3, *nanopores* were fabricated with assistance of NBs, as first reported in our previous study [3] and later by Janda et al [4]. When PS films were immersed in water, small bubbles

---

Corresponding authors:
Yuliang Wang: wangyuliang@buaa.edu.cn & Detlef Lohse: d.lohse@utwente.nl

disappear with time and generate nanopores on sample surfaces [3]. Similar results were also reported on graphene surfaces [5]. Recently, by applying negative pressure, Janda et al. obtained nano pinholes and nano protrusions, respectively, on thinner and thicker PS films, respectively. The NB caused generation of nanostructures on PS surfaces is mostly due to the presence of surface forces at the three phase contact line and the high inner pressure of NBs [6].

Through experiments, we found that the type of NB assisted nanostructures is strongly related to two factors, namely the NB size and the thickness of the PS films. Nanostructures tend to form namely on ultrathin PS films (with thickness from 3 nm to 7 nm). This is mostly because the polymer chain entanglement density is greatly reduced with decreasing sample thickness, as motivated theoretically [7, 8] and shown experimentally [9, 10]. This will lead to a much lower elastic modulus and fracture strength of ultrathin PS films as compared to their bulk values. During our experiments, smaller NBs (less than 50 nm in diameter and thus with much higher inner pressure, assuming constant contact angle) mostly disappear and lead to formation of nanopores on ultrathin PS film with thickness around 3 nm. Bigger NBs (larger than 80 nm) last longer and will lead to the formation of nanoindents, even on a relative thick PS film.

Sample 3 was first immersed into DI water and smaller NBs (with width less than 50 nm) were formed on the surface. After that, NBs disappeared and a porous PS surface was obtained. Water was then removed from the sample and the sample was kept in an vacuum chamber for 4 h to remove the remaining water. The experiment in fluid was performed to study NB nucleation.

AFM Measurement

A commercial AFM (Resolve, Bruker) operating in tapping mode was used for imaging the sample in both air and deionized (DI) water. A silicon cantilever (NSC36/ALBS, MikroMasch) with a quoted tip radius of 8 nm and stiffness of 0.6 N/m from the manufacturer was used for the scanning in air and DI water. The measured resonance frequencies of the cantilever in air and water were about 55 KHz and 16 KHz, respectively. While imaging in air and liquid, the drive frequencies were slightly lower than that of the selected resonance. A scan rate of 2 Hz with a 0° scan angle was used. All experiments were performed at an ambient environment (temperature: 26 ± 1 °C).

In all three experiments, the sample surfaces were first scanned in air by tapping mode AFM (TMAFM). Then they were immersed into DI water to perform liquid imaging. The image scanning began immediately within 10 minutes after immersing the surface into water. For sample 1, the scanning lasted for more than 5 hours. For sample 2, the scanning lasted for more than 10 hours. The free oscillation amplitude of the cantilever at working frequency was about 290 mV. The larger setpoint oscillation amplitude of about 280 mV (namely 96.5% of free amplitude) was applied for liquid imaging to minimize disturbance of AFM tips to NBs.

As mentioned above, nanopits of different sizes were obtained on PS films. For sample 1, the distributions of the nanopits' width and depth are shown in **Figure S1(a)** and **S1(b)**, respectively. The nanopit width distributed from 50 nm to 100 nm. The nanopit depth mostly changed in between 1 to 6 nm. There was one nanopit with a depth of 12 nm, which reached down to the silicon substrate. Figure S1(a) shows the correlation between width and depth.

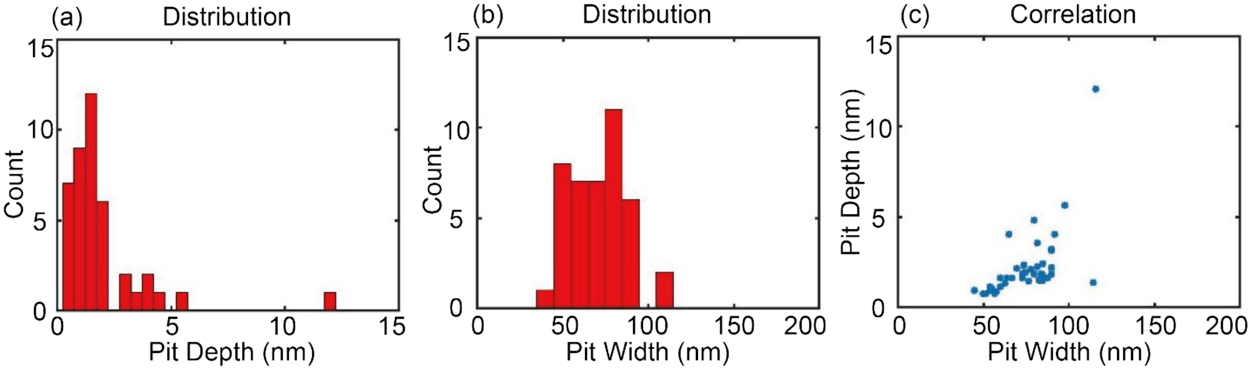

Figure S1 Width and depth distribution of nanopits on sample 1. *(a) Histogram of nanopit widths on sample 1. The nanopit width changed from 40 nm to 110 nm. (b) Histogram of nanopit depths on sample 1. The nanopit depths distributed from 1 nm to 6 nm. The correlation between width and depth is shown in (c).*

In the analysis of **Figure 1**, we found that three NBs remained on their initial locations around a large nanopits after NB coalescence. In the area selected by a green dashed box in **Figure 1(c)**, one can see that the three NBs remained after NB coalescence. **Figure S2** shows the zoom-in mesh plots of the selected area in **Figure 1(a-c)**. As mentioned in the main manuscript, this is thought to be due to the existence of the large nanopit in the selected area, providing strong pinning sites.

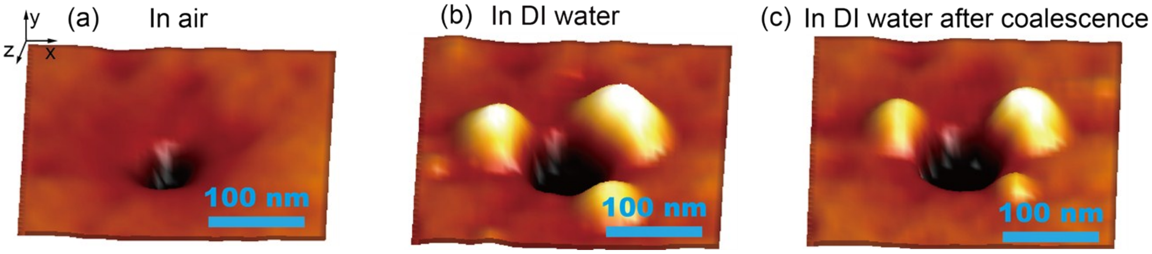

Figure S2 A deep and large nanopit on sample 1. *3D mesh plots of the same areas selected in Figure 1. One can clearly see the topography of the nanopit in air (a), in DI water (b), and after coalescence (c).*

For sample 2, the distributions of nanopits' width and depth are shown in **Figure S3(a)** and **S3(b)**, respectively. On the sample, one can see that the nanopit widths mainly distributed from 50 nm to 250 nm. The nanopit depths distributed in two sections, 3-4 nm, and 10-13 nm. For the nanopits of which depth located in the section section (10-13 nm), they reached down to the bottom of the silicon substrate.

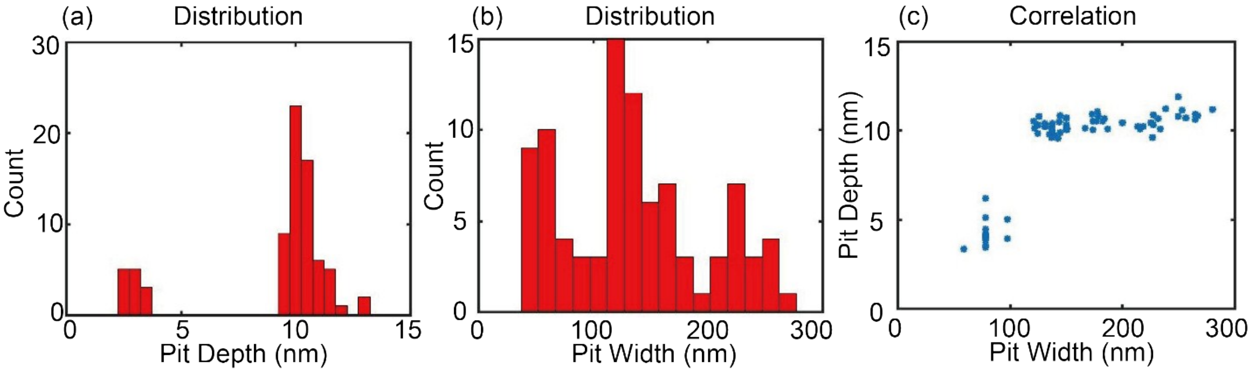

Figure S3 Width and depth distribution of nanopits on sample 2. *(a) Histogram of nanopit widths on sample 2. The nanopit widths mainly changed from 50 nm to 250 nm. (b) Histogram of nanopit depths on sample 2. The nanopit depths distributed in two sections, 3 – 4 nm, and 10-13 nm. (c) Corrrelation of width and depth.*

Nanobubble Verification Experiment

Studies on surface NBs have been suffering from artifacts for years as explained in [11, 12]. For the samples used in this study, there are potentially three kinds of artifacts, namely solid particles, liquid objects [12], and blisters [13]. To value out such artifacts, several experiments were designed and conducted to verify that the spherical objects we observed were indeed NBs. In this supporting information, we report the result of several verification experiment.

Nanobubble Coalescence Experiment

The nanobubble coalescence experiment was performed to distinguish nanobubbles from solid particles and blisters. It is well known that nanobubbles can move and coalesce to generate larger ones under higher scan load [1, 14, 15]. However, blisters and solid objects cannot coalesce. In this study, we performed NB coalescence experiment on PS samples. The result for one of these experiments is show in **Figure S4**. **Figure S4(a)** is a height image of the sample surface obtained with 96% setpoint value in TMAFM after the sample was immersed into DI water. One can see that nanobubbles with width about 100 nm were obtained on the sample surface. To conduct coalescence experiment, we first apply 80% setpoint to scan the area. After that, the area was rescanned with 96% setpoint. The resulting image is shown in **Figure S4(b)**. One can see that nanobubbles with much larger size were obtained with reduced density. If the spherical objects were solid particles or blisters, they could not be coalesced in this way. Therefore, one can conclude that the spherical-cap like objects were neither solid particles, nor blisters.

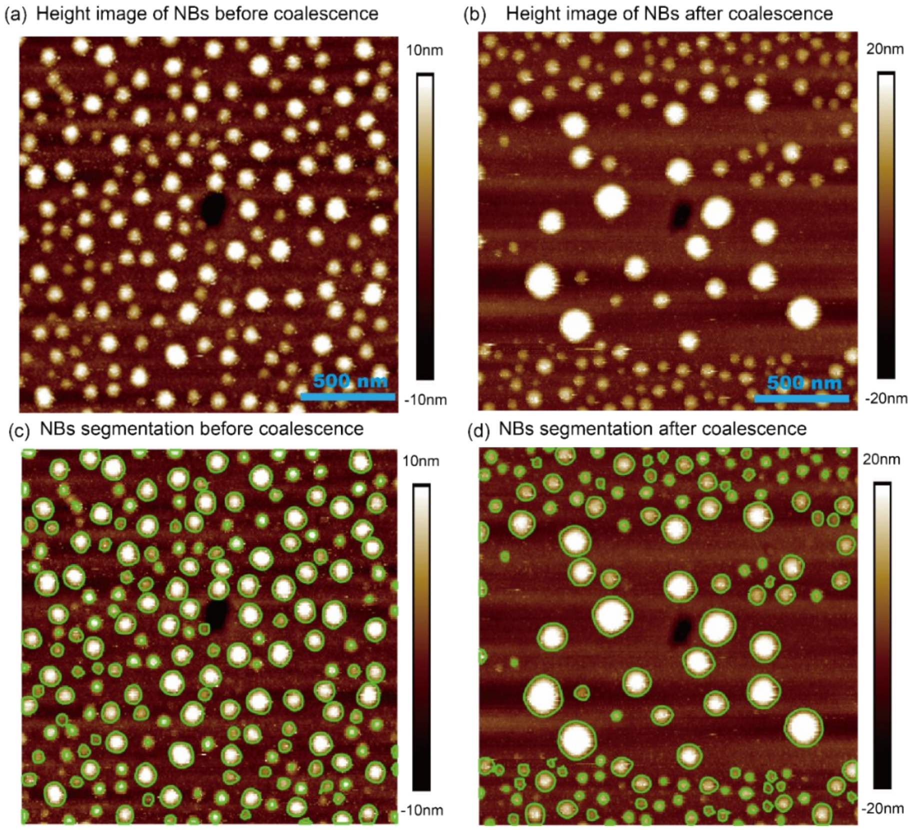

Figure S4*. Nanobubble coalescence performed on a PS surface. (a) AFM height image of the sample surface after immersed into DI water. (b) AFM height image of the same area after a higher scan load was applied. Nanobubbles at lower number density, but much larger size were obtained, indicating nanobubble coalescence. (c-d) NB image segmentation for NB height images in (a) and (b), respectively. The green contours are detected NB boundaries with a homemade NB segmentation algorithm.*

Moreover, the NB volumes before and after the coalescence were measured with a home-made NB image segmentation algorithm [15]. To do so, the AFM images of the NBs were first segmented. The results are shown in **Figure S4(c)** and **S4(d)** for NB images shown in **Figure S4(a)** and **S4(b)**, respectively. With the segmented NB images, the NB volumes were calculated. The total volumes of NBs in **Figure S4(a)** and **S4(b)** are about 3.7×10^6 nm^3 and 7.1×10^6 nm^3, respectively. The obtained result is in a good agreement with what we reported recently [15]. The increased NB volume after NB coalescence may partly be explained by the reduced Laplace pressure in the larger NBs, and partly be by diffusion of dissolved gas into the merging process. A quantitative analysis of these two effects is beyond the scope of the present paper.

Tip-Sample Interaction Experiments

The second approach to distinguish NBs from solid particles and blisters is an amplitude-distance curve measurement above the spherical-cap-like objects. During extension or retraction motion of an oscillating tip relative to a NB, the amplitude of the tip shows gradually decreases with reducing tip-sample separation distance [14, 16]. However, the oscillating amplitude of AFM tips rapidly decreases once they get into contact with surfaces of solid particles or blisters, very different from the behavior of nanobubbles. One example of the amplitude-distance curve of AFM obtained on a spherical-cap like object is given in **Figure S5**. **Figure S5(a)** is an AFM height image of the PS sample surface (sample 1). In the center area, there is a big spherical-cap-like object. We measured amplitude-distance curves on the object and obtained two kinds of curves. Here we took amplitude-distance curves obtained at two selected points (marked as 1 and 2). The results are shown in **Figure S5(b)**.

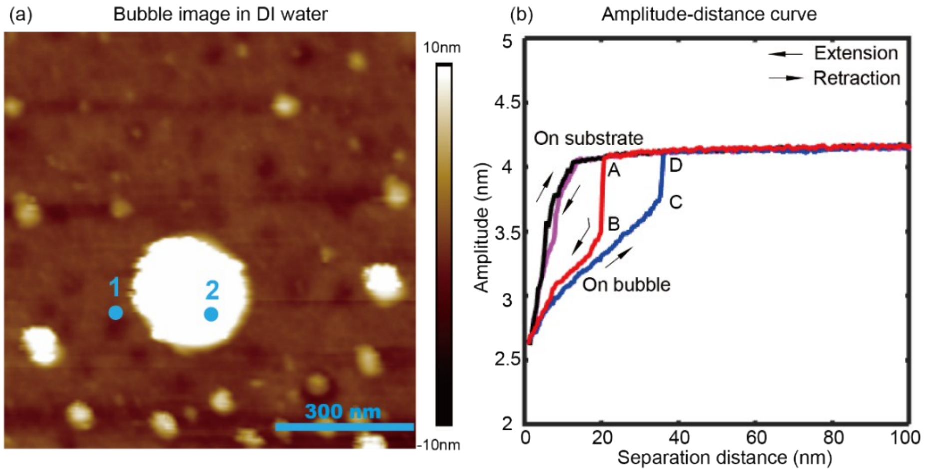

Figure S5. *Amplitude-distance curve measurement on a spherical-cap like object and sample substrate. (a) AFM height image of the sample surface in DI water, showing a big spherical-cap like object in the center. (b) Two typical amplitude-distance curves measured at point 1 and 2, respectively.*

One kind of curve is the one obtained above the substrate (point 1 in **Figure S5(a)**). Once the tip contacts the substrate, the amplitude rapidly decreases with decreasing tip-sample separation distance. The other kind of curve is the one obtained above the spherical-cap like domains (point 2 in **Figure S5(a)**). One can see that the obtained result is consistent with the one of our recent investigation [16]. As described there [16], there are typical snap-in period A → B and detached period C → D, which corresponds to the position where the AFM tip gets and loses contact with the object, respectively. The tip-sample interaction further confirms that the obtained spherical-cap like objects were not solid ones, neither blisters.

Degassing Experiments

To distinguish NBs from liquid contamination (PDMS droplets, for example), we applied degassing experiments[12, 17, 18]. For a PS sample, we first imaged the sample surface in air. The image is shown in **Figure S6(a)**. One can see that the surface is flat without any spherical-cap like objects. After that, the sample was immersed into DI water. We first obtained spherical-cap like objects on the sample surface, as shown in **Figure S6(b)**. Then, the AFM liquid cell with the sample immersed in water was transferred into a vacuum chamber to degas the water for over 4 hours. After that, the liquid cell was brought back to AFM and was re-scanned. The result is shown in **Figure s6(c)**. One can see that the spherical-cap like objects had all disappeared. This implies that the observed spherical-cap like objects were actually gas bubbles and not droplets of a poorly solvable liquid.

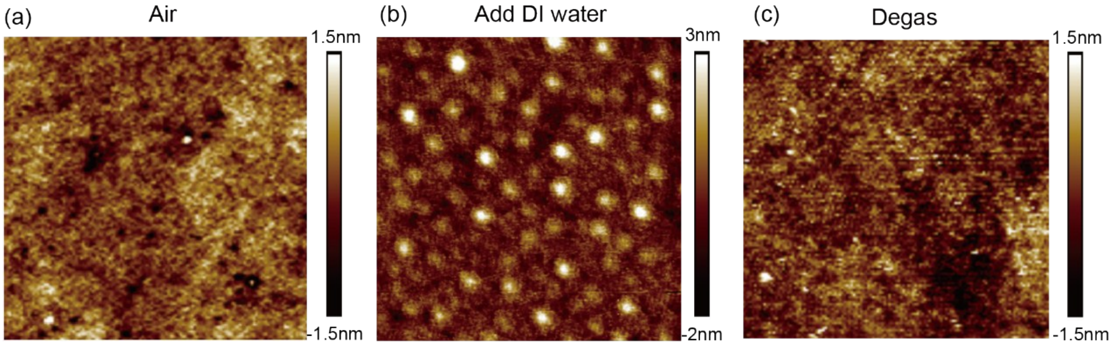

Figure S6 *Degassing experiment. (a) A PS sample surface obtained with tapping mode AFM in air. (b) Spherical-cap like objects obtained on the sample surface after it was immersed into DI water. (c) AFM height image of the same sample after the liquid cell (the sample remained in water during degassing) was kept for 4 hours in a vacuum chamber for degassing. The NBs have dissolved.*

Deconvolution of Tip Radius and Correction of NB Contact Angles

It is well known that a topography image obtained from an AFM is actually the convolution of the AFM tip and substrate morphologies [19-21]. Therefore, the measured NB width needs to be corrected due to the finite size of the cantilever tip radius. In the case of the spherical-cap-liked

NBs, the influence of the AFM tip on the contact angles of the protruding NBs is illustrated in **Figure S7a**. In the figure, the dashed cross section is the directly measured one from AFM images, while the solid one is the NB's actual cross section. From the figure, one can see that the tip radius causes overestimation of the NB width. The deconvolution of the AFM tip gives a corrected expression of the NB radius, width, and contact angle, namely[19-21]

$$R_{\mathrm{c}}' = \frac{(D)^2 + 4H^2}{8H} - R_{tip}, \tag{S1}$$

$$D' = \sqrt{D^2 - 8HR_{tip}}, \tag{S2}$$

and

$$\theta' = 2\arctan(2H / D'), \tag{S3}$$

where D' and D, θ' and θ, R_c' and R_c, H' and H ($H' = H$) are the actual and apparent (uncorrected) values of width, contact angles, radius of curvature, and height of the NB, respectively, and R_{tip} is the tip radius (about 8 nm in this case).

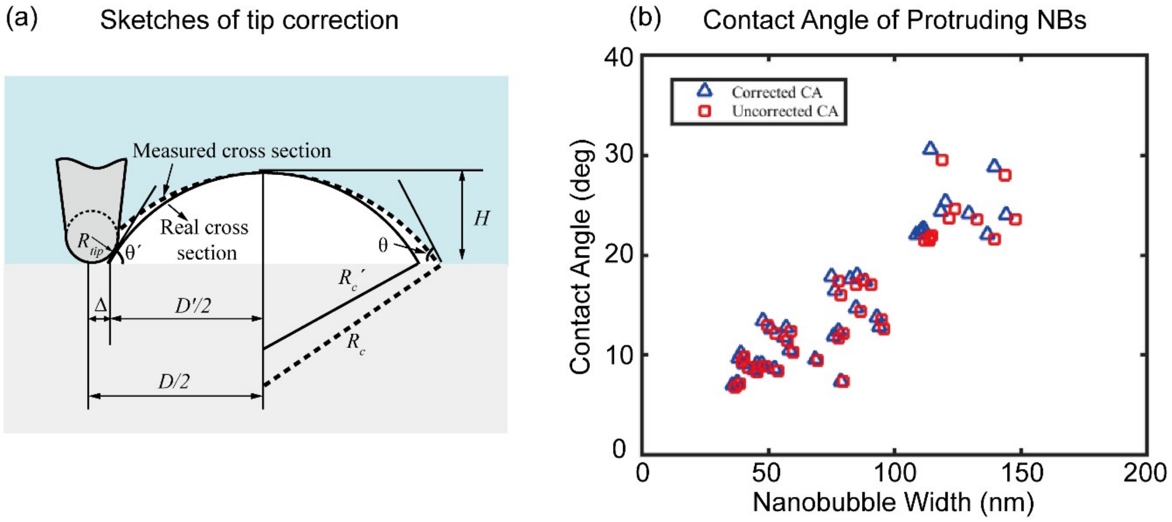

Figure S7 *(a) Schematic sketch of the NB size correction through deconvolution of the tip radius. (b) Comparison of the corrected and uncorrected contact angle (CA) for protruding NBs. The difference between the corrected contact angle and uncorrected ones is slight.*

With **Eq. (S3)**, NB contact angle can be corrected. For the NBs with width of 50-150 nm, we found that D is about 2-4 nm larger than D'. A comparison of the corrected and uncorrected contact angle of NBs is conducted to evaluate the effect of finite size of tip radius on contact angle measurement, as shown in **Figure S7b**. From the result, one can see that the uncorrected CA is slightly lower (about 2%) than that of the corrected one.

The classification of planar and protruding NBs is based on the value of their contact angles. The distribution of contact angles for all trapped NBs is shown in **Figure S8**. In this study, the NBs with contact angles of 0º or even slightly less are referred to as planar NBs. The others are protruding NBs, of which contact angles are normally larger than 10 º.

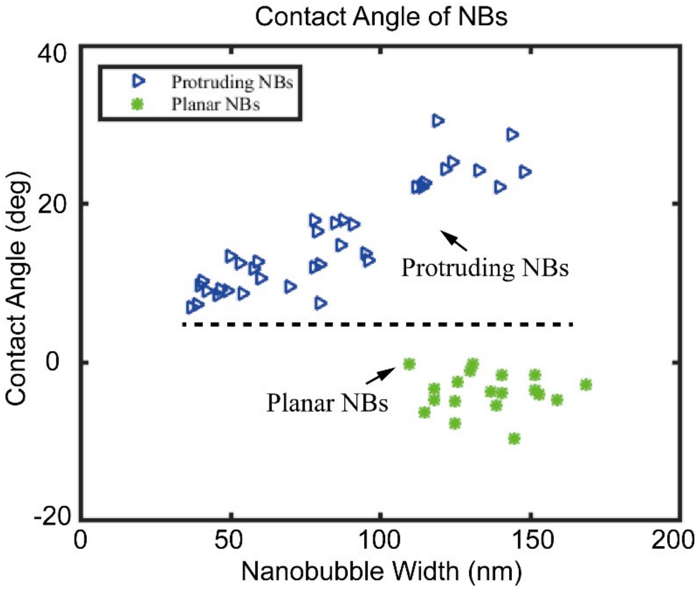

Figure S8 *Corrected contact angles for all trapped NBs (planar and protruding). The contact angle for planar NBs is mostly less than 0º. The dashed horizontal line in the figure divides the trapped NBs into two categories: protruding and planar NBs.*

References:

1. Y. Wang, B. Bhushan and X. Zhao, *Langmuir*, 2009, **25**, 9328-9336.
2. G. Reiter, *Langmuir*, 1993, **9**, 1344-1351.
3. Y. Wang, B. Bhushan and X. Zhao, *Nanotechnology*, 2009, **20**, 045301.
4. H. Tarabkova and P. Janda, *Journal of Physics-Condensed Matter*, 2013, **25**, 184001.
5. P. Janda, O. Frank, Z. Bastl, M. Klementova, H. Tarabkova and L. Kavan, *Nanotechnology*, 2010, **21**, 095707.
6. J. H. Weijs, B. Andreotti and J. H. Snoeijer, *Soft Matter*, 2013, **9**, 8494-8503.
7. H. R. Brown and T. P. Russell, *Macromolecules*, 1996, **29**, 798-800.
8. H. Meyer, T. Kreer, A. Cavallo, J. P. Wittmer and J. Baschnagel, *Eur. Phys. J.-Spec. Top.*, 2007, **141**, 167-172.
9. L. Si, M. V. Massa, K. Dalnoki-Veress, H. R. Brown and R. A. L. Jones, *Phys. Rev. Lett.*, 2005, **94**, 127801.
10. J. H. Lee, J. Y. Chung and C. M. Stafford, *Acs Macro Letters*, 2012, **1**, 122-126.
11. D. Lohse and X. Zhang, *Rev. Mod. Phys.*, 2015, **87**, 981-1035.
12. R. P. Berkelaar, E. Dietrich, G. A. M. Kip, E. S. Kooij, H. J. W. Zandvliet and D. Lohse, *Soft Matter*, 2014, **10**, 4947-4955.
13. R. P. Berkelaar, P. Bampoulis, E. Dietrich, H. P. Jansen, X. H. Zhang, E. S. Kooij, D. Lohse and H. J. W. Zandvliet, *Langmuir*, 2015, **31**, 1017-1025.

14. B. Bhushan, Y. Wang and A. Maali, *J. Phys.: Condens. Matter*, 2008, **20**, 485004.
15. Y. Wang, H. Wang, S. Bi and B. Guo, *Beilstein Journal of Nanotechnology*, 2015, **6**, 952-963.
16. Y. Wang, H. Wang, S. Bi and B. Guo, *Scientific Reports*, 2016, **6**, 30021.
17. L. Bao, Z. Werbiu, D. Lohse and X. Zhang, *J. Phys. Chem. Lett.*, 2016, **7**, 1055-1059.
18. L. J. Zhang, Y. Zhang, X. H. Zhang, Z. X. Li, G. X. Shen, M. Ye, C. H. Fan, H. P. Fang and J. Hu, *Langmuir*, 2006, **22**, 8109-8113.
19. B. M. Borkent, S. de Beer, F. Mugele and D. Lohse, *Langmuir*, 2010, **26**, 260-268.
20. D. Li and X. Zhao, *Colloid Surf. A-Physicochem. Eng. Asp.*, 2014, **459**, 128-135.
21. B. Song, W. Walczyk and H. Schoenherr, *Langmuir*, 2011, **27**, 8223-8232.